UNIVERSITY OF DEBRECEN
FACULTY OF MEDICINE
DEPARTMENT OF OPERATIVE TECHNIQUES AND SURGICAL RESEARCH

Renal Ne/De tumor cells and related microcirculatory changes in a rat model

Scientific Research Essay

Ho Quang Tri Vinh
6th Year Medicine

Supervisors:

Ádám Attila Mátrai MSc

Dr. Ádám Deák DVM, PhD

I agree to submit this thesis:

Ádám Attila Mátrai
PhD student
supervisor

Dr. Ádám Deák
assistant professor
supervisor, SRS advisor

Prof. Dr. Norbert Németh
head of Department

Debrecen, 2025

Table of Contents

Abstract

Introduction: The development of malignant tumors and their abnormal vasculature may result in severe alterations in tissue perfusion. The aim of this study was to investigate the alterations in the kidney microcirculation, related micro-rheological changes, and parenchymal structural differences in a rat-origin mesenchymal mesoblastic nephroma (Ne/De) tumor cell implantation model.

Materials and Methods: Sixteen female Fischer-344 rats (bodyweight: 190.17±4.96 g) were anesthetized (3% isoflurane) (permission reg. nr.: 21/2017/UDCAW), the retroperitoneum was opened in the lumbar region. The left kidney was exposed and the Gelaspon® disc containing 0.9 % NaCl or tumor cells ($1x10^6$ Ne/De tumor cells, established by Prof. Dr. Pál Kertai) was placed under the renal capsule. The wound was closed in two layers. The microcirculation of the kidney was monitored by Cytocam IDF camera on the 1st and the 9th postoperative (p.o.) days. Blood samples were taken on the day of implantation, and on the 4th and 9th p.o. days for testing hematological parameters, red blood cell (RBC) deformability and aggregation.

Results: Leukocyte count significantly increased by the 4th p.o. day ($p=0.002$ vs. base) followed by a decrease on day 9 ($p=0.002$ vs. day 4). Platelet count increased on p.o. days 4 and 9 ($p<0.001$ vs. base). In all RBC aggregation index values a continuous and significant increase was observed (M5 index value on 4th day: $p=0.034$, on 9th day: $p<0.001$ vs. base; M10 index values on 4th day: $p=0.034$, on 9th day: $p=0.008$ vs. base). The RBC deformability describing parameter $SS_{1/2}$ [Pa] was remarkably increased on day 9 ($p=0.007$ vs. base), representing worsened RBC deformability. On day 9 the structural features of the tumor tissue and a heterogenous blood flow pattern were detected by the Cytocam compared to healthy or to the contralateral intact kidney. Vessels with abnormal geometry and shape were often seen in the recordings, where flow parameters were increased, while in other territories RBC aggregates and microcirculatory deterioration was observed.

Conclusion: The growing malignant renal tumor caused significant deterioration and heterogeneity in the microcirculation, of which background can be the abnormal vessels and impaired blood micro-rheology. The model seems to be suitable for further investigations of tumor growth and related microcirculatory changes

List of abbreviations

CT: computed tomography

EI: elongation index

EI_{max}: maximum elongation index

Hct: hematocrit

Hgb: hemoglobin

IDF: incident dark field

MCH: mean corpuscular hemoglobin

MCHC: mean corpuscular hemoglobin concentration

MCV: mean corpuscular volume

Ne/De: mesoblastic nephroma tumor cell line

PPV: proportion of perfused vessels

RBC: red blood cell

SS: shear stress

$SS_{1/2}$: shear stress at half maximum EI

WBC: white blood cell

1. Introduction

Malignant tumors' biology is characterized by the formation of atypical vasculatures that cause significant impact on tissue perfusion. The vasculature in tumors is markedly distinct from that of heathy tissues, including structural, geometric and functional abnormalities. Tumor vessels are often disorganized, unevenly distributed, dilated and more permeable than in normal tissue. This results in impaired and irregular blood flow (Figure 1) (Schaaf et al., 2018).

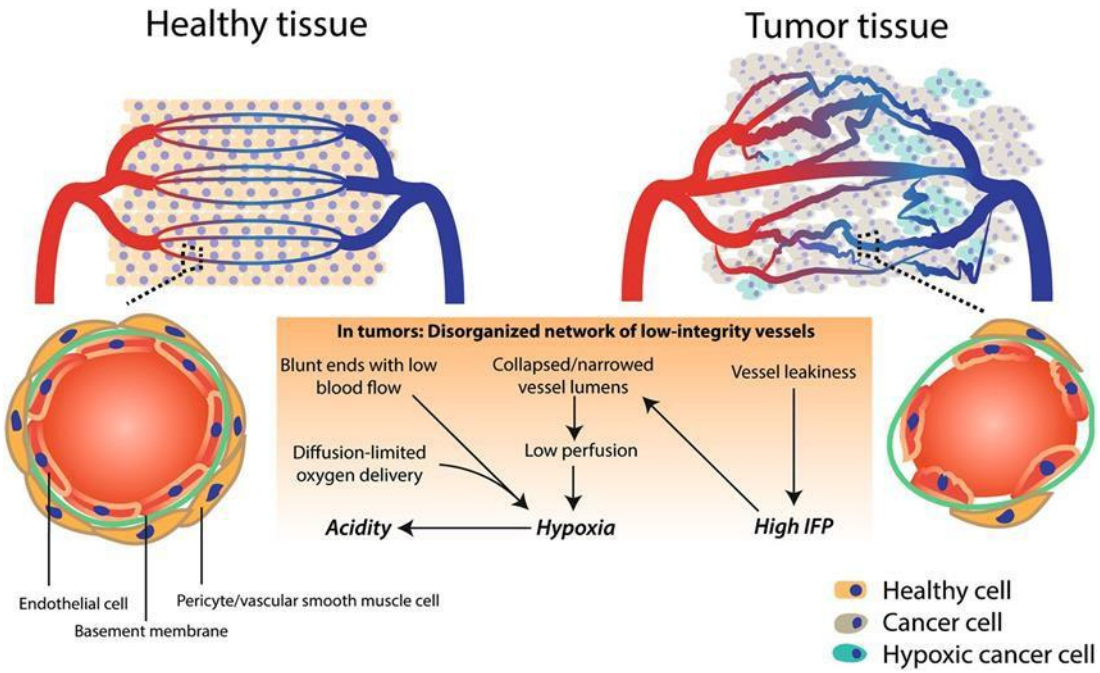

Figure 1. Vascular structure in normal vs. tumor tissue. (Upper left panel) In normal tissue, a well-organized vasculature network is often seen. (Lower left panel) These vessels are mature, with endothelial cells surrounded by a basement membrane and pericytes, and tight intercellular junctions. (Upper right panel) In tumors, blood vessels are chaotic, with low pericyte coverage and loose junctions, leading to leaky vessels and increased interstitial fluid pressure. (Lower right panel) This causes some tumor regions to become hypoxic (indicated in green), which causes the surrounding microenvironment to be more acidic (Schaaf et al., 2018)

These alterations of the blood vessels lead to significant micro-circulatory and micro-rheological changes, including impaired red blood cell (RBC) deformability and increased RBC aggregation, and cause a compromise in blood perfusion. This in turn forms a vicious feedback loop where diminished blood flow exacerbates tissue hypoxia, mechanical trauma to blood cells, and the production of free radicals, further impairing microcirculatory function (Figure 2) (Nemeth et al., 2018).

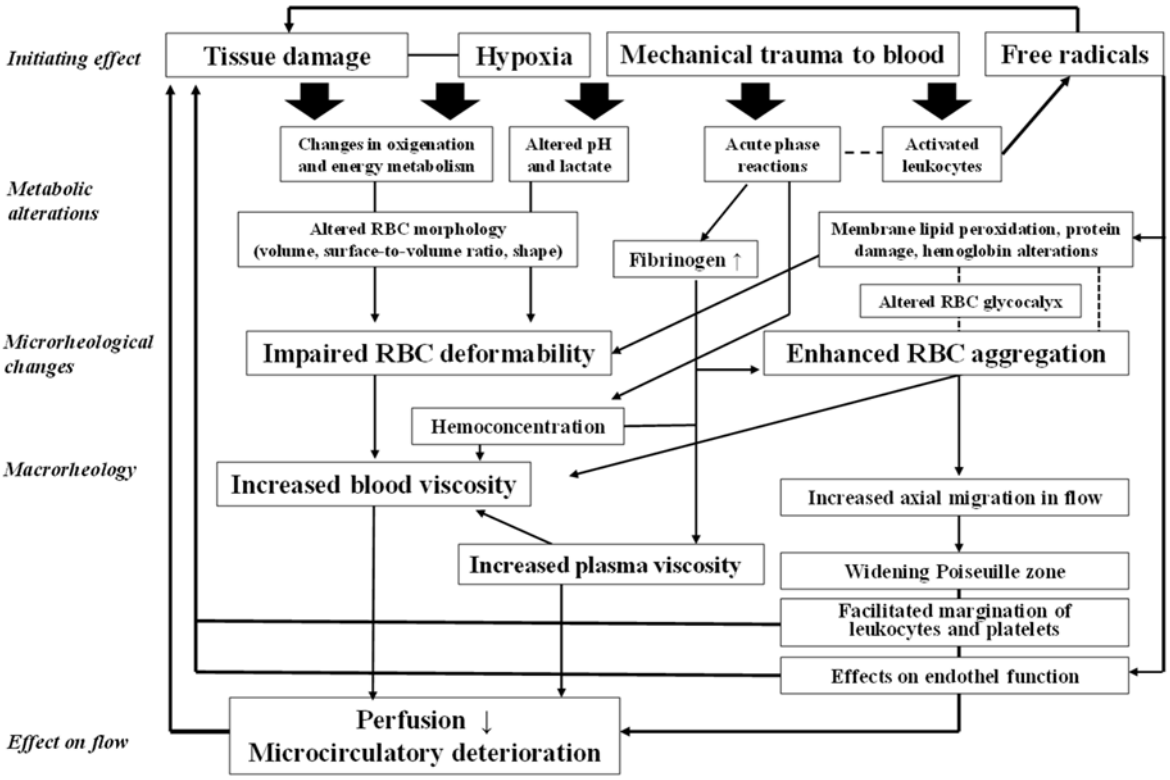

Figure 2. Initiating factors including tissue hypoxia, mechanical trauma to blood cells, and free radicals cause red blood cell micro-rheological changes in the tissue, leading to decreased perfusion. This in turns creates a vicious cycle that worsens the initiating factors. (Nemeth et al., 2018)

One of the primary consequences of impaired tumor perfusion is the formation of hypoxic conditions. Hypoxia plays an important role in the promotion of tumor aggressiveness (Esteves et al., 2021; Li et al., 2021), and the resistance to cancer treatments such as radiotherapy (Jordan and Sonveaux, 2012a; Kleibeuker et al., 2016). Radiotherapy turns oxygen in the tumor tissue into free radicals that cause damage to the tumor DNA (Wardman, 2007; Fuchs-Tarlovsky, 2013). In hypoxic conditions, the production of these free radicals is significantly reduced, causing poorer therapeutic outcomes (Hughes et al., 2019; Majidpoor and Mortezaee, 2021a). Furthermore, hypoxia has been shown to promote tumor invasiveness as well as metastasis, causing difficulties in controlling the tumor (Wang et al., 2020; Qian et al., 2023a).

The vasculature within solid tumors plays a crucial role not only in tumor growth, but also in the efficacy of cancer therapeutic interventions. The abnormalities in vessels' structure, permeability and chaotic organization leads to poor tumor tissue perfusion, which contributes to the poor delivery of therapeutic agents into the tumor (Jordan and Sonveaux, 2012b; Tian et al., 2017; Xu et al., 2018). In normal tissues, well-organized blood vessels ensure even drug distribution, but in tumors, the chaotic vascular architecture acts as a barrier, limiting the penetration of the drugs into the tumor core. This results in suboptimal concentrations of

chemotherapeutic agents within the tumor, allowing cancer cells to survive and eventually develop resistance (Majidpoor and Mortezaee, 2021b). Moreover, high interstitial pressure also opposes the flow of therapeutic agents from the bloodstream into the tumor tissue, which further complicates the drug delivery (Bertrand et al., 2014).

In the face of these challenges, the concept of vascular normalization has gained some attention as a promising therapeutic strategy, aimed at temporary restoration of abnormal tumor vasculature to improve blood flow and to enhance the efficacy of treatments (Qian et al., 2023b). By temporarily normalizing the abnormal tumor vasculature into a more organized state, better perfusion can be achieved, and the delivery of chemotherapeutic agents can be improved. This strategy has been shown to improve hypoxia, enhance immune cell infiltration, and possibly restore the tumors' sensitivity to chemotherapy as well as radiotherapy (Jain, 2005; Theek et al., 2018; Qian et al., 2023a).

Inflammatory processes, which are often present in tumor environments, can lead to changes in RBC aggregation and deformability, which all lead to increased blood viscosity (Szentkereszty et al., 2014). Many factors have been shown to influence the red blood cells and hemorheology. In static conditions, erythrocytes form aggregates with a face-to-face morphology called Rouleaux formation. RBCs also have deformability, allowing the cells to passively change shape in response to shearing and compression in the vessels. RBCs' deformability is influenced by the absolute volume of red blood cells, morphology of red blood cells, surface-volume ratio, intracellular viscosity), cell membrane viscosity and elasticity (Baskurt and Meiselman, 2003; Baskurt et al., 2009a).

The study of tumor vasculature and its effect on microcirculation is key to understanding the complex progression of malignancies and their physiological consequences. Kidney tumors like mesoblastic nephroma, a rare pediatric neoplasm, serve as a useful model for studying tumor-related microcirculatory alterations. The tumor is characterized by its aggressive nature, high mitotic activity, and the tendency to invade surrounding tissues (Dezso et al., 1990; Trencsenyi et al., 2009; Kepes et al., 2022). These factors provide a suitable framework for investigations of tumor-related vascular anomalies, metastasis, and microcirculatory alterations.

2. Aim

The primary objective of this study is to investigate the alterations in the kidney microcirculation, related micro-rheological changes, and parenchymal structural differences in a rat-origin mesenchymal mesoblastic nephroma (Ne/De) tumor cell implantation model. By studying these parameters, we aim to uncover more about the relationship between tumor progression and the dysfunction of microcirculation. This can potentially provide a foundation for future research into therapeutic interventions that can target the abnormalities of tumors' vasculature.

3. Materials and methods

The experiments were performed in accordance with the European Union Directive and National Regulations and with the approval of the University of Debrecen Committee of Animal Welfare (reg. Nr.: 21/2017/UDCAW)

3.1. Animal model

The study was performed using 16 female Fischer-344 rats (bodyweight: 190.17±4.96 g, aged 6 to 6.5 months old), which were divided into two groups: the Ne/De group (n=8) and the sham-operated group (n=8).

3.2. Tumor cell implantation

Gelaspon® sheets were used to create disks with a diameter of 4 mm and a thickness of 1 mm. A defined number of mesoblastic nephroma cells (1 x 10^6 Ne/De tumor cells, established by Prof. Dr. Pál Kertai) were suspended in physiological saline solution and placed onto the Gelaspon® disks. Dulbecco's Modified Eagle Medium (DMEM) containing 10% fetal bovine serum was used for the cultivation of Ne/De cells, which was supplemented with a 1% antimycotic-antibiotic solution. The monolayer cell cultures were maintained in T-75 cell culture flasks containing 12ml of medium, in an incubator providing 5% CO2 and 95% humidity (ESCO CCl-170B-8 incubator) at 37C. The cultures were passaged 3 times per week. Control disks were prepared with only a physiological saline solution (0.9 %NaCl).

3.3. Surgical Procedure

All rats were anesthetized with 3% isoflurane gas prior to surgical procedures. Anesthesia was maintained throughout the experiment to ensure the welfare of the animals. The retroperitoneum was opened made in the lumbar region through an abdominal section, exposing the left kidney. The Gelaspon® disk was carefully placed beneath the capsule of the left kidney. The surgical wound was closed in two layers (Figure 3).

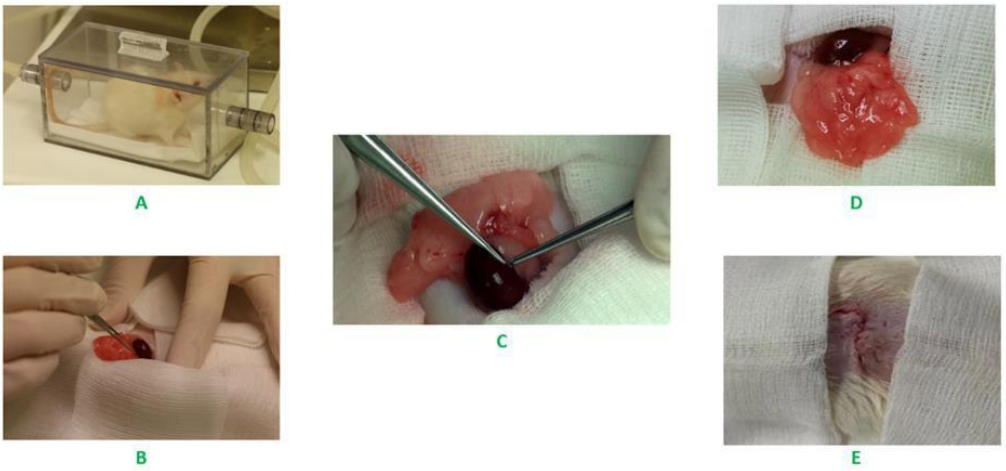

Figure 3. Surgical procedure to place Gelaspon® disks under the renal capsule. All rats were first anesthetized with 3% isoflurane gas (A); Left kidney was exposed through an abdominal incision (B); Gelaspon® disk was placed under the renal capsule (C); The kidney was replaced (D) and the wound was closed in two layers (E).

3.4. Blood sampling protocol

Blood samples were collected from the lateral tail veins of the rats on the day of implantation, as well as on the 4th and 9th postoperative (p.o) days, to test hematological parameters, red blood cell (RBC) deformability, and aggregation.

3.5. Computer Tomography

Post-operative imaging was performed using computer tomography (CT) scans on both coronal and trans-axial planes to assess tumor growth and kidney morphology. The positioning of the rats during CT scans was ventral, with the animals lying on their abdomen.

3.6. Microcirculation monitoring

The kidney's microcirculation was monitored using a CytoCam IDF camera (Braedius Medical B.V., Netherlands) on the 1st and 9th day postoperative days. The CytoCam IDF camera is a pen-like device equipped with 12 green LEDs at the tip. This device illuminated the specimen, and the scattered light captured by the camera sensor was used to produce video recordings of microcirculatory dynamics (Figure 4) (van Elteren et al., 2015). This device allowed for detailed investigation and comparison of vessel architecture, perfusion, and vascular changes in both tumor and normal tissue.

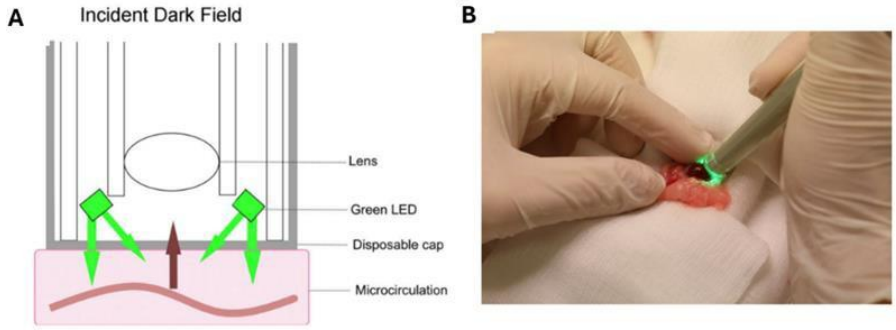

Figure 4. Schematic illustration describing the mechanism of the Cytocam IDF camera; 12 green LEDs at the tip of the device illuminate the microcirculation; the scattered light passes through the lens and is captured by the camera sensor; images of the microcirculation are recorded in the device's software (van Elteren et al., 2015) (A); The kidney tissue and the adjacent tumor tissue are visualized using the Cytocam camera (B).

3.7. Hematological Assessments

We used the Sysmex K-4500 microcell counter (TOA Medical Electronics Co., Ltd., Kobe, Japan) to take measurements for red blood cell count (RBC [T/L]), hematocrit (Hct [%]), mean corpuscular volume (MCV [fL]), mean corpuscular hemoglobin (MCH [pg]), mean corpuscular hemoglobin concentration (MCHC [g/dL]), platelet count (Plt [G/L]), white blood cell count (WBC [G/L]), and hemoglobin concentration (Hgb [g/dL]).

3.8. Red blood cell deformability

A LoRRca Maxsis Osmoscan ektacytometer (Mechatronics BV, Netherlands) was used to assess erythrocyte deformability (Baskurt et al., 2007; Baskurt et al., 2009b). This device places the blood samples under shear stress, and measures the red blood cell elongation through laser diffraction. The elongation index (EI) is calculated based on the shear stress (SS), which ranges from 0.3 to 30 Pa. In the standard deformability analysis, 2 mL of a polyvinylpyrrolidone-phosphate-buffered saline (PVP–PBS) solution was mixed with 10 μL blood sample.

3.9. Determination of erythrocyte aggregation

A Myrenne MA-1 aggregometer (Myrenne GmbH, Roetgen, Germany) was utilized to measure the aggregation index from blood samples. The aggregometer uses the light transmittance photometric method, which assesses the red blood cell aggregation by analyzing the changes in light transmission through the blood sample over time. The measurement required 20 μL of blood, which was first disaggregated with controlled shearing at a shear rate of 600 s^{-1}. Following this, light transmission was measured for 5, or for 10 seconds either at stasis or under low shear conditions (Baskurt et al., 2009c; Vayá et al., 2009). All measurements were performed at room temperature (20–25 °C) (Lee et al., 2007; Baskurt et al., 2009c; Vayá et al., 2009).

3.10. Histological analysis

Histological slides were made using hematoxylin and eosin (H&E) staining to assess and compare histological structures of both normal tissue and tumor tissue. Tissue samples were initially fixed in formalin, embedded in paraffin, sectioned, and subsequently stained using the standard H&E protocol. The thickness of the histological sections was 5μ. Slide scanning was performed using the VENTANA DP200 slide scanner (Hoffmann-La Roche, Roche Holding AG, Basel, Switzerland).

3.11. Statistical analysis

Statistical analysis was performed utilizing the SigmaStat Software version 3.1.1.0 (Systat Software Inc., San Jose, CA, USA). Data are displayed as means ± standard deviation (S.D.). Data were analyzed using repeated measures ANOVA or the Friedman test, Student's t-test or the Mann–Whitney rank sum test. A p-value of less than 0.05 was considered statistically significant for all comparisons.

4. Results

4.1. Computer Tomography (CT)

In the sham-operated group on the 9th p.o. day, the coronal plane CT scan revealed that the left kidney was of normal size when compared to the contralateral right kidney, indicating the absence of any abnormal mass growth in the left kidney. In contrast, the Ne/De group showed significant changes on the 9th p.o day. The coronal and trans-axial CT images showed substantial tumor growth in the left kidney (Figure 5).

Figure 5. Computer Tomography (CT) scan in trans-axial plane in tumor implanted group. Clearly visible tumor mass behind the left kidney. K: kidney, T: tumor

4.2. Hematological parameters

The results showed a significant change in white blood cell (WBC) count in both the sham-operated and Ne/De group. A marked increase in WBC count was observed at 4 days post-operation, followed by a subsequent decline after 9 days post-operation. This increase was noticeably more pronounced in the Ne/De group, suggesting a strong systemic immuneresponse to the tumor growth. Red blood cells' parameters including hemoglobin concentration,red blood cell count, and hematocrit, saw lower levels at the 4 day p.o point when compared tothe Ne/De group. By day 9, these values in both groups showed a progressive increase relativeto the baseline and to the 4-day p.o levels. The sham-operated group exhibited lower values atthe 4-day post-operative mark when compared to the tumor-implanted group. However, by day9, these parameters showed a progressive increase in both groups relative to baseline and 4-daypost-operative levels (Figure 6).

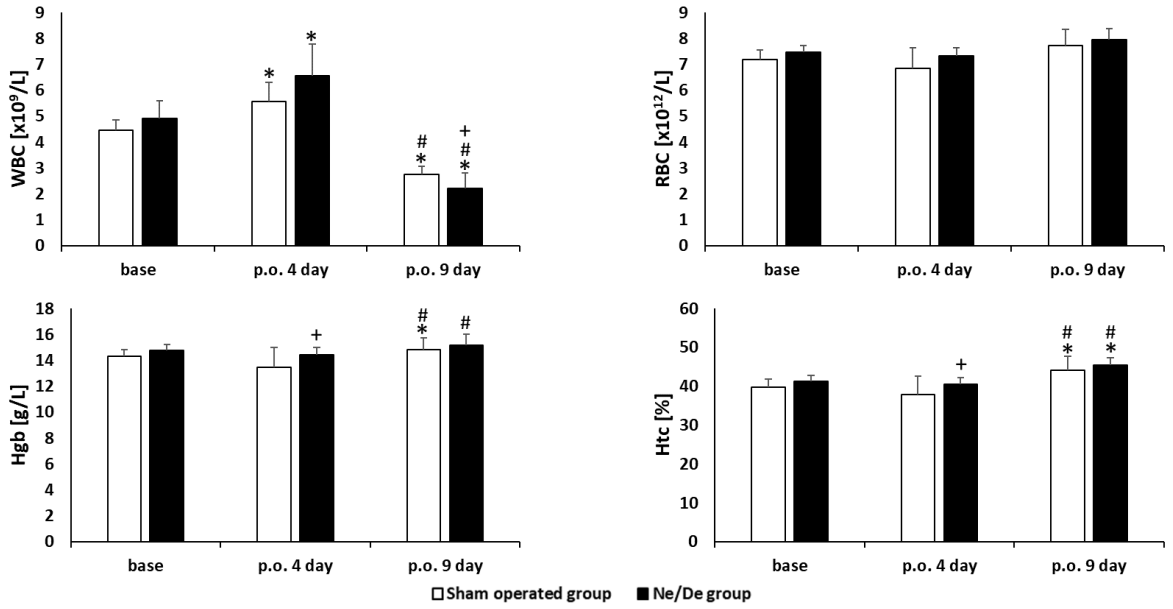

Figure 6. Hematological parameters of Sham operated group and Ne/De group on the day of the operation (base), 4 days post-operatively, and 9 days post-operatively; Means ± S.D ; $p < 0.05$, * vs. base, # vs. p.o. 4 day, + vs. Sham operated group

Mean Corpuscular Volume (MCV) displayed a noticeable increase in both groups by the 9th post-operative day. The Mean Corpuscular Hemoglobin (MCH) and Mean Corpuscular Hemoglobin Concentration (MCHC) both showed a decline across the 9-day observation period in both experimental groups. Moreover, a significant increase in platelet count was observed on both day 4 and day 9 post-operation in both groups (Figure 7).

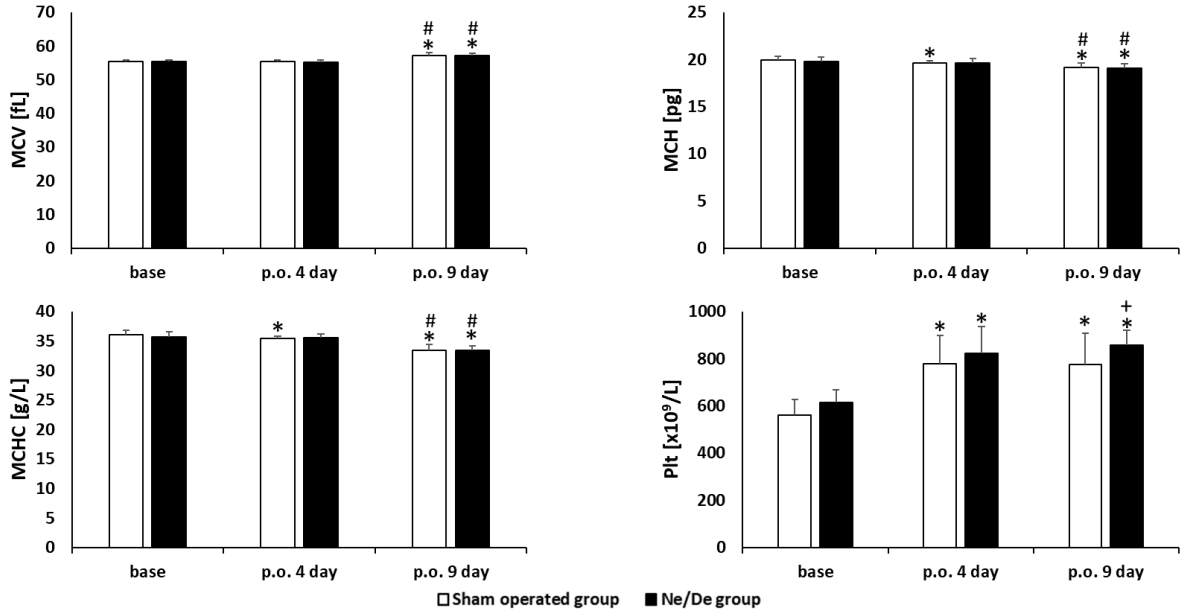

Figure 7. Mean corpuscular volume, mean corpuscular hemoglobin, mean corpuscular hemoglobin concentration and platelet count on the day of the operation (base), 4 days post-operatively, and 9 days post-operatively; Means ± S.D, $p < 0.05$, * vs. base, # vs. p.o. 4 day, + vs. Sham operated group

4.3. Red blood cell deformability:

On the 9th post-operative day, the RBC deformability in the sham operated group showed significant improvements, particularly at low shear stress (3 Pa). In contrast, the tumor-implanted Ne/De group after 9 days exhibited reduced deformability under low shear stress conditions, while deformability improved under high shear stress (Figure 8).

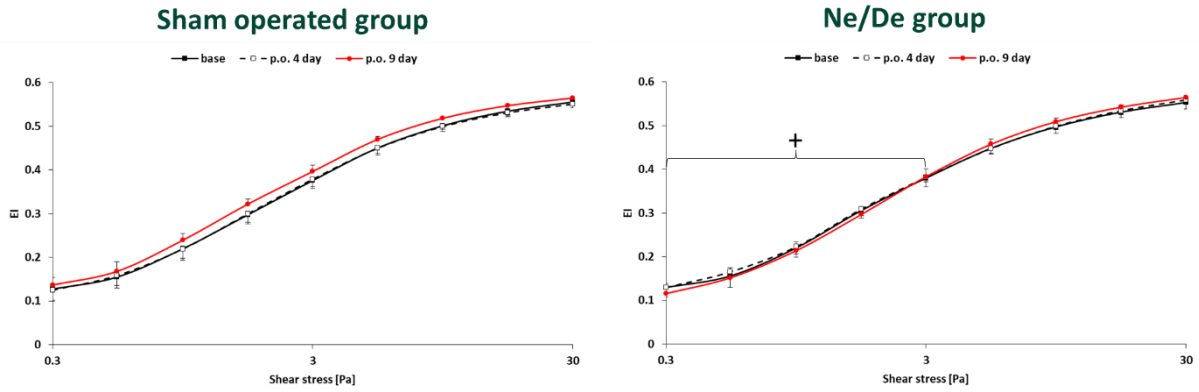

Figure 8. Elongation index-shear stress curve in the Sham operated group and Ne/De group on the day of the operation (base), 4 days post-operatively, and 9 days post-operatively. Means ± S.D, $p < 0.05$, + vs. Sham operated group

The maximum elongation index (EI_{max}) increased significantly in both groups by the 9th post-operative day, indicating enhanced RBC flexibility. However, the shear stress required to achieve half of the EI_{max} ($SS_{1/2}$) increased only in the Ne/De group, suggesting impaired deformability under lower stress. The ratio of EI_{max} to $SS_{1/2}$ was calculated, further revealing differences in deformability dynamics between the groups. These findings suggest a tumor-induced change in RBC mechanical properties in the Ne/De group (Figure 9).

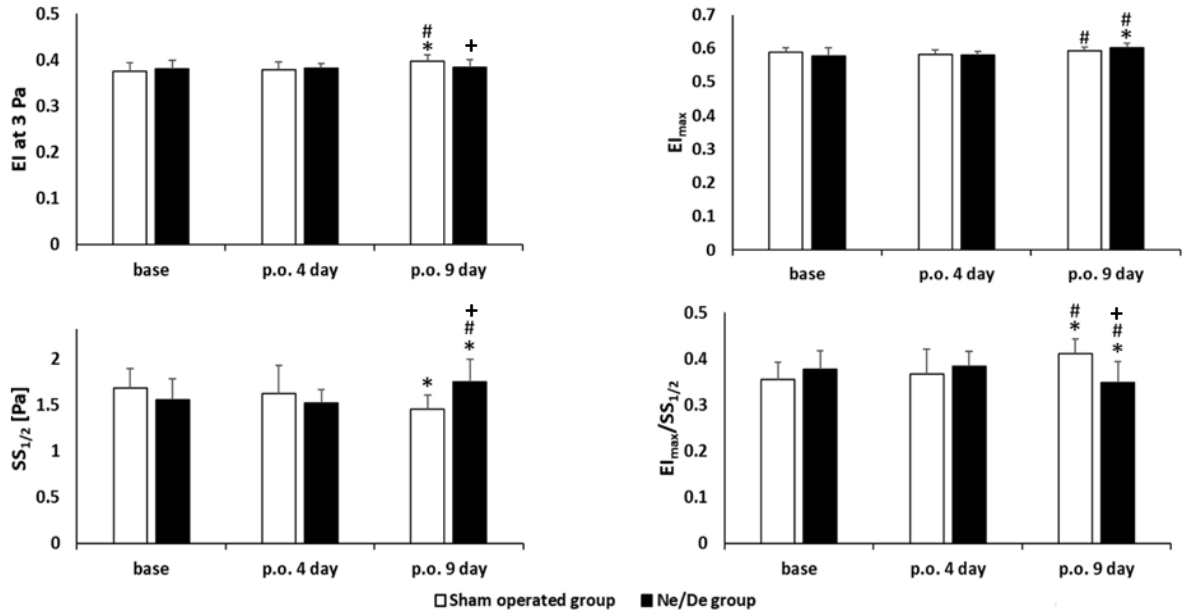

Figure 9. Elongation index at 3Pa, maximal elongation index, shear stress required to achieve half of the EI_{max}, and ratio between EI_{max} and (EI max/ SS1/2) measured in the Sham operated group and Ne/De group on the day of the operation (base), 4 days post-operatively, and 9 days post-operatively; Means ± S.D, $p < 0.05$, * vs. base, # vs. p.o. 4 day, + vs. Sham operated group

4.4. Red blood cell aggregation

The Ne/De group showed a substantial increase in RBC aggregation by the 9th post-operative day, most notably in the M and M1 values under 10-second measurement conditions. These changes were significantly higher than in the sham-operated group, reflecting enhanced RBC clumping in the tumor environment. The increased aggregation in the Ne/De group suggests a systemic response to tumor growth, potentially contributing to microcirculatory impairments observed in this study (Figure 10).

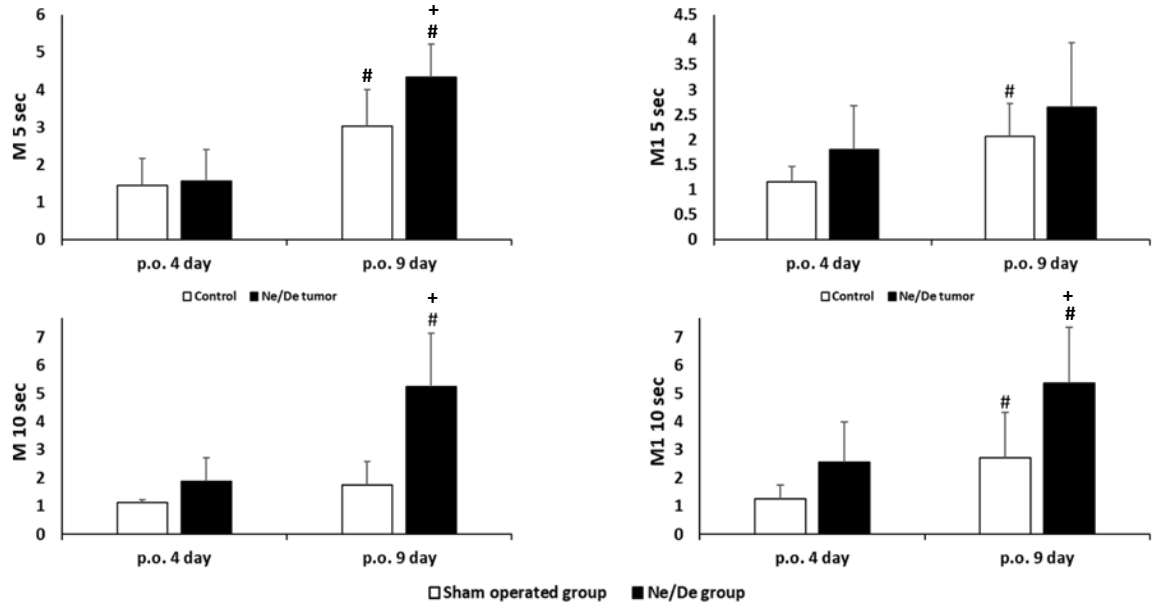

Figure 10. Relative to base value measured for 5 or 10 seconds either at stasis (M values) or under low shear conditions (M1 values); Means ± S.D, $p < 0.05$, # vs. p.o. 4 day, + vs. Sham operated group

4.5. Renal microcirculation

The microcirculation of the kidney was assessed using a Cytocam IDF device on the first and last day of the experiment by recording videos from the normal kidney, the sham-operated kidney, the kidney tissue adjacent to the tumor, and the tumor bearing kidney itself. In the normal kidney and the sham-operated kidney, microvascular architecture appeared highly organized, with well-defined arterioles and venules that were evenly distributed throughout the tissue. There were no signs of vessel dilation, indicating healthy perfusion and structured blood flow. In contrast, the tumor-bearing kidney and the kidney tissue adjacent to the tumor showed a significant disarray in microvascular architecture. Vessels appeared disorganized and chaotic, with arterioles and venules being irregularly distributed and markedly dilated. This abnormality was most pronounced in the tumor itself, where the vasculature displayed severe structural disruption. Software analysis of the Cytocam IDF device revealed that the Proportion of Perfused Vessels (PPV) showed significant increase in the kidney with the tumor compared to the other groups (Figure 11).

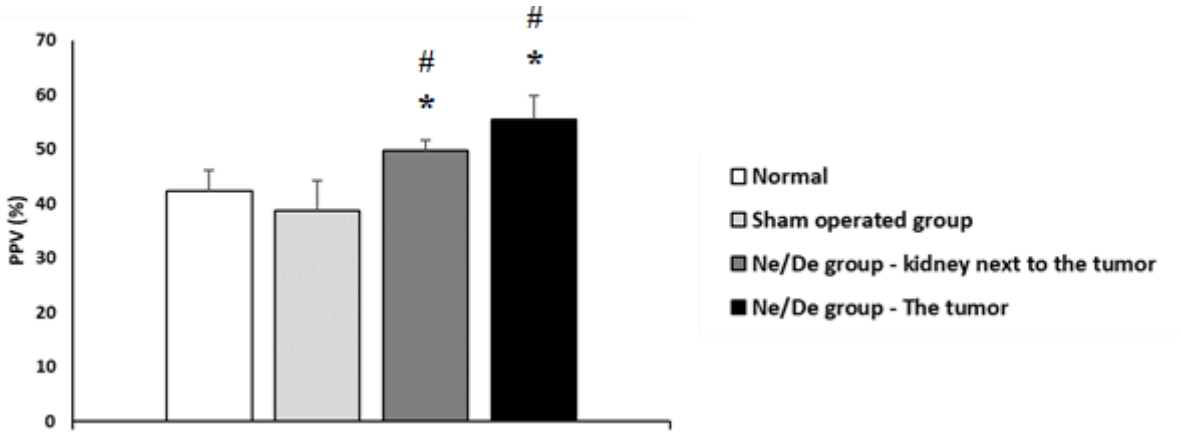

Figure 11. Proportion of Perfused vessels (PPV) of the normal kidney, the sham-operated group kidney, the kidney next to the tumor and in the tumor; Means ± S.D, $p < 0.05$, * vs. Normal, # vs. Sham operated group

4.6. Histology

Hematoxylin and Eosin (H&E) staining was used to generate histological slides. This staining clearly makes the demarcation between normal and malignant renal tissues, allowing for easy differentiation (Figure 12). Furthermore, a significant presence of mitotic figures and unusual mitotic activity is apparent, indicating aggressive tumor cell growth. Infiltration of adipose tissue into the renal parenchyma is noted, compromising the normal tissue architecture. Moreover, the renal tubules are surrounded by atypical tumor cells, demonstrating the degree of tumor infiltration into the kidney's structural elements.

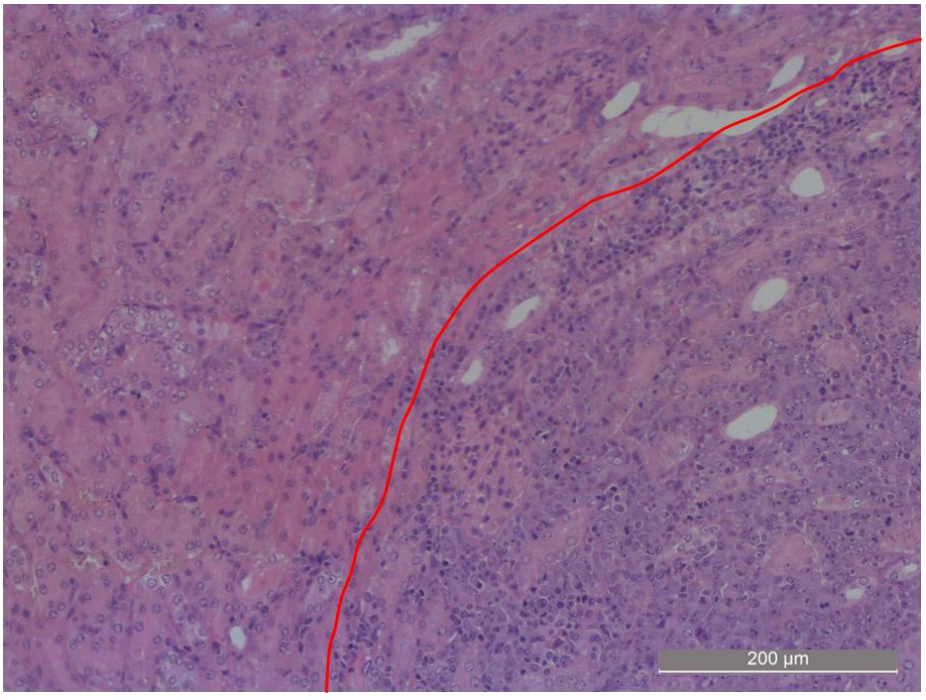

Figure 12. Histological section of tumors kidney. The red line marks the border between normal and tumor renal tissue.Stain: Hematoxylin and eosin; magnification: 200×.

5. Discussion

In our study, CT imaging confirmed substantial tumor growth in the left kidney. The tumor-implanted group exhibited a significant spike in WBC count at 4 days post-surgery, which decreased by day 9. Other hematological values all show an increase in 4 days and 9 days post-operative, apart from the Mean corpuscular Volume and Mean Corpuscular hemoglobin concentration which show a decrease in both groups. RBC aggregation considerably decreased, with increased M and M1 values seen in the tumor group. Red blood cell deformability enhanced in both the sham-operated and Ne/De groups under high shear stress at day 9, evidenced by an elevated elongation index at 3 Pa and an increased EI_{max}, whilethe tumor group's $SS_{1/2}$ also increased on day 9. Normal kidney blood circulation shows well- organized, clearly defined arterioles and venules. In contrast, the tumor-implanted groups exhibit chaotic, disorganized vessels with ill-defined, unevenly distributed, and dilated arterioles and venules.

The observed micro-rheological changes in the tumor-implanted kidneys, characterized by increased viscosity and reduced red blood cell deformability, are crucial for understanding their implications on tissue perfusion. Increased plasma viscosity can significantly impair micro-circulatory blood flow by slowing the transit time of red blood cells through the capillaries, resulting in compromised tissue blood flow and impaired tissue perfusion (Ruiz et al., 2013). Increased plasma viscosity also hinders fluid motion in microcirculation, which are important sites for energy dissipation (Metry et al., 2011). Additionally, the reduced deformability of RBCs in the tumor-bearing models may be caused by oxidative stress and inflammation, which are known to damage the RBC membrane cytoskeleton, reducing the cell flexibility and capillary transit (Pretorius, 2018). These micro-rheological alterations are well aligned with our understanding of tumor biology, which indicates that these changes in blood flow can form a favorable environment for tumor progression and survival. One of the prominent features of such an environment is hypoxia, which is impaired oxygen delivery. This triggers adaptive responses in the tumor tissue, including the upregulation of hypoxia-inducible factors (HIFs) and raised levels of vascular endothelial growth factor (VEGF). These responses promote angiogenesis and abnormal vessel formation, promoting tumor growth and facilitate immune evasion and resistance to chemotherapeutic drugs (Yi et al., 2019; You et al., 2021). In addition to VEGF, chronic hypoxia induces the expression of genes and metabolic shifts that are beneficial to the tumor cells, such as the Warburg effect, and allows tumor cells to thrive under low oxygen conditions (Hirschhaeuser et al., 2011; Korbecki et al., 2021a, 2021b). This

altered metabolism further worsens the local microenvironment, increasing lactic acid production and potentially cause impact on vascular tone and permeability. (Hirschhaeuser et al., 2011; Pérez-Tomás and Pérez-Guillén, 2020).

These findings create significant practical implications in cancer treatment. Interventions aimed at improving RBC deformability or improving blood viscosity could enhance tissue perfusion and decrease the tumor growth. It has been suggested that fluid resuscitation strategies can influence blood rheology, which indicates that therapies focusing on blood viscosity may enhance the efficacy of current cancer treatments (Guerci et al., 2014). Thus, the interaction between micro-rheological alterations and tumor biology highlights the significance of considering these findings to improve current therapeutic options in cancer treatment. Drugs like pentoxifylline, which enhances RBCs' deformability, or antioxidants that protect them from damage, could be used as adjuvants in treatments for kidney tumors (Muravyov et al., 2011; Słoczyńska et al., 2013; Radosinska and Vrbjar, 2021; Steele et al., 2024). Additionally, controlling blood rheology could potentially improve drug delivery by enhancing perfusion and reducing hypoxia-mediated resistance mechanisms, similar to strategies like sonopermeation, which use ultrasound waves to improve drug delivery for better therapeutic access. (Snipstad et al., 2018).

In addition to sonopermeation, other therapeutic strategies that aim to enhance drug delivery are increasingly being explored for tumor treatments. One such approach is vascular normalization, which includes anti-VEGF therapy or angiotensin receptor blocker that can temporarily restore the blood flow efficiency in tumors. These methods reduce vessel leakiness and interstitial pressure, thereby improving drug penetration. For instance, bevacizumab, an anti-VEGF therapy, has been shown to change blood vessel permeability in tumors, helping chemotherapy to be more effective in melanoma models (Turley et al., 2012). Anti-VEGF therapy has also been demonstrated to enhance CAR-T cell delivery and efficacy in glioblastoma by normalizing tumor vasculature (Dong et al., 2023). Similarly, angiotensin inhibition has been shown to decompress tumor blood vessels, which improves drug delivery and enhances the chemotherapy efficacy (Chauhan et al., 2013). Furthermore, enzymatic disruption of the tumor surrounding environment, such as using hyaluronidase to lyse the tumor extracellular matrix, can improve drug delivery into tumor tissue (Whatcott et al., 2011). Techniques like electroporation, which temporarily opens cell membranes using electrical pulses, also show potential in increasing intracellular drug uptake by solid tumors (Tsoneva et al., 2022). These methods, especially when combined with improved rheological properties,

could greatly improve treatment results in kidney tumors by helping drugs reach the tumor more effectively.

The mesoblastic nephroma rat model (Ne/De) has demonstrated significant potential as a platform suitable for exploring tumor growth and associated microcirculatory alterations. Unlike the more commonly studied models of solid tumors, such as breast or colorectal cancer, the kidneys are significantly more vascularized. This special characteristic leads to unique structural and functional changes of the tissue in response to tumor development, making this model highly suitable for examining tumor growth and the associated microvascular adaptation (Szabo et al., 2022). The crucial difference of this model compared to other models is its focus on an organ that already has substantial blood flow and filtration function. This provides a unique environment for examining the adaptation of the tumor's microcirculation to meet increased metabolic demands, and its interaction with the tissue's complex blood filtration and excretion functions. Such interaction has been shown to significantly influence tumor behavior (Oxburgh, 2022). Additionally, because kidneys typically have a high perfusion rate, even small changes in vessel structure or blood viscosity can greatly affect how well oxygen and nutrients are delivered (Sugimori et al., 2013). As such, the Ne/De model offers a useful systemto study how tumors change surrounding vasculature not only for growth, but also for long- term survival and immune evasion. This makes it especially suitable for preclinical testing of therapies that target tumor vasculature or drug delivery.

Thus, the Ne/De model is a suitable system for studying not only tumor-induced changes in microcirculation but also how these changes affect normal organ function. The Ne/De model offers unique advantages over other tumor models. Firstly, it allows for microvascular adaptation specific to kidney physiology. While many tumor models explore the broad aspects of angiogenesis and perfusion changes, the Ne/De model allows for detailed insights into microvascular adaptations that are specific to renal anatomy and physiology. Secondly, the Ne/De model has demonstrated changes in red blood cell deformability and aggregation, which are micro-rheological parameters. These findings offer a more focused exploration of how rheological changes caused by the tumor impact tissue perfusion. In many other tumors models this aspect is often left understudied, focusing instead on vessel density and perfusion without considering how altered blood flow dynamics contribute to tissue hypoxia and resistance to treatment. Lastly, the histopathological findings in the Ne/De model present similarly to human renal tumors, particularly the observed parenchymal changes such as fibrosis and extracellular matrix remodeling (Wang et al., 2014). This model allows researchers to explore how these changes impact both tumor progression and the surrounding healthy tissue on a histological

level. Given these attributes, the Ne/De model is particularly suitable for further studies focused on the interaction between tumor growth and microcirculatory changes. This model not only allows for the investigation of tumor-induced vascular remodeling and its consequences on organ function but also provides a basis for exploring therapeutic approaches that aim to counteract these changes. Further research could explore gene expression changes in the endothelial cells of tumor-bearing kidneys, particularly those related to hypoxia, angiogenesis, and oxidative stress. This would help us better understand how tumors alter blood vessels at the molecular level. By studying microvascular and micro-rheological alterations, researchers can develop strategies to modulate blood flow properties, improve oxygen delivery, and potentially control tumor growth through enhanced vascular function. Furthermore, the model's unique focus on kidney-specific changes offers a valuable foundation for developing targeted therapies in renal tumor pathology.

6. Conclusion

The malignant renal tumor caused significant deterioration and alterations in the microcirculation, which can be explained by the presence of abnormal vessels and impaired blood micro-rheology. These findings highlight the complex interaction between tumor growth and microvasculature, underlying the role of vascular abnormalities and altered hemorheology in the progression of tumors.

This model proves to be suitable for further investigations into the pathophysiology of tumor growth and related microcirculatory changes. It provides a valuable basis for exploring the mechanisms behind vascular dysfunction caused by tumors, and for assessing potential therapies that enhance microcirculation.

7. Acknowledgement

I would like to give my heartfelt gratitude to my two supervisors Ádám Attila Mátrai and Dr. Ádám Deák, who introduced me to the topic as well as provided invaluable guidance throughout the writing of this thesis. Furthermore, I would like to thank Professor Dr. Norbert Németh, head of Department, and members of the Department of Operative Techniques and Surgical Research, head and members of the Department of Nuclear Medicine and Translational Imaging and head and members of the Department of Pathology for providing me with technical support, state-of-the-art facilities, and continuous guidance in a professional environment.

I would like to also thank my loved ones for their unconditional love and support throughout my academic career. Their support and advice have given me unyielding strength to endure and overcome all the challenges and hurdles I have encountered along the way.

8. Reference

1. Baskurt, O.K., Boynard, M., Cokelet, G.C., Connes, P., Cooke, B.M., Forconi, S., Liao, F., Hardeman, M.R., Jung, F., Meiselman, H.J., Nash, G., Nemeth, N., Neu, B., Sandhagen, B., Shin, S., Thurston, G., Wautier, J.L., International Expert Panel for Standardization of Hemorheological Methods, 2009a. New guidelines for hemorheological laboratory techniques. Clin. Hemorheol. Microcirc. 42, 75–97.
2. Baskurt, O.K., Hardeman, M.R., Rampling, M.W., 2007. Handbook of Hemorheology and Hemodynamics. IOS Press.
3. Baskurt, O.K., Hardeman, M.R., Uyuklu, M., Ulker, P., Cengiz, M., Nemeth, N., Shin, S., Alexy, T., Meiselman, H.J., 2009b. Parameterization of red blood cell elongation index--shear stress curves obtained by ektacytometry. Scand. J. Clin. Lab. Invest. 69, 777–788.
4. Baskurt, O.K., Meiselman, H.J., 2013. Data reduction methods for ektacytometry inclinical hemorheology. Clin. Hemorheol. Microcirc. 54, 99–107.
5. Baskurt, O.K., Meiselman, H.J., 2003. Blood rheology and hemodynamics. Semin. Thromb. Hemost. 29, 435–450.
6. Baskurt, O.K., Uyuklu, M., Ulker, P., Cengiz, M., Nemeth, N., Alexy, T., Shin, S., Hardeman, M.R., Meiselman, H.J., 2009c. Comparison of three instruments for measuring red blood cell aggregation. Clin. Hemorheol. Microcirc. 43, 283–298.
7. Bertrand, N., Wu, J., Xu, X., Kamaly, N., Farokhzad, O.C., 2014. Cancer Nanotechnology: The impact of passive and active targeting in the era of modern cancer biology. Adv. Drug Deliv. Rev. 66, 2–25.
8. Chauhan, V.P., Martin, J.D., Liu, H., Lacorre, D.A., Jain, S.R., Kozin, S.V., Stylianopoulos, T., Mousa, A.S., Han, X., Adstamongkonkul, P., Popović, Z., Huang, P., Bawendi, M.G., Boucher, Y., Jain, R.K., 2013. Angiotensin inhibition enhances drug delivery and potentiates chemotherapy by decompressing tumour blood vessels. Nat Commun 4, 2516.
9. Dezso, B., Rady, P., Morocz, I., Varga, E., Gomba, S., Poulsen, K., Kertai, P., 1990. Morphological and immunohistochemical characteristics of dimethylnitrosamine-induced malignant mesenchymal renal tumor in F-344 rats. J. Cancer Res. Clin. Oncol. 116, 372–378.
10. Dong, X., Ren, J., Amoozgar, Z., Lee, S., Datta, M., Roberge, S., Duquette, M., Fukumura, D., Jain, R.K., 2023. Anti-VEGF therapy improves EGFR-vIII-CAR-T cell delivery and efficacy in syngeneic glioblastoma models in mice. J Immunother Cancer 11, e005583.

11. Esteves, M., Monteiro, M.P., Duarte, J.A., 2021. The effects of vascularization on tumor development: A systematic review and meta-analysis of pre-clinical studies. Crit. Rev. Oncol. Hematol. 159, 103245.
12. Fuchs-Tarlovsky, V., 2013. Role of antioxidants in cancer therapy. Nutr. Burbank Los Angel. Cty. Calif 29, 15–21.
13. Guerci, P., Tran, N., Menu, P., Losser, M.-R., Meistelman, C., Longrois, D., 2014. Impact of fluid resuscitation with hypertonic-hydroxyethyl starch versus lactated ringer on hemorheology and microcirculation in hemorrhagic shock. Clin. Hemorheol. Microcirc. 56, 301–317.
14. Hirschhaeuser, F., Sattler, U.G.A., Mueller-Klieser, W., 2011. Lactate: a metabolic key player in cancer. Cancer Res 71, 6921–6925.
15. Hughes, V.S., Wiggins, J.M., Siemann, D.W., 2019. Tumor oxygenation and cancer therapy—then and now. Br. J. Radiol. 92, 20170955.
16. Jain, R.K., 2005. Normalization of tumor vasculature: an emerging concept in antiangiogenic therapy. Science 307, 58–62.
17. Jordan, B.F., Sonveaux, P., 2012a. Targeting tumor perfusion and oxygenation to improve the outcome of anticancer therapy. Front. Pharmacol. 3, 94.
18. Jordan, B.F., Sonveaux, P., 2012b. Targeting Tumor Perfusion and Oxygenation to Improve the Outcome of Anticancer Therapy1 3.
19. Képes, Z., Barkóczi, A., Szabó, J.P., Kálmán-Szabó, I., Arató, V., Garai, I., Árkosy, P., Jószai, I., Deák, Á., Kertész, I., Hajdu, I., Trencsényi, G., 2022. In Vivo Assessments of Mesoblastic Nephroma (Ne/De) and Myelomonoblastic Leukaemia (My1/De) Tumour Development in Hypercholesterolemia Rat Models. Int. J. Mol. Sci. 23, 13060.
20. Kleibeuker, E.A., Fokas, E., Allen, P.D., Kersemans, V., Griffioen, A.W., Beech, J., Im, J.H., Smart, S.C., Castricum, K.C., van den Berg, J., Schulkens, I.A., Hill, S.A., Harris, A.L., Slotman, B.J., Verheul, H.M., Muschel, R.J., Thijssen, V.L., 2016. Low dose angiostatic treatment counteracts radiotherapy-induced tumor perfusion and enhances the anti-tumor effect. Oncotarget 7, 76613–76627.
21. Korbecki, J., Kojder, K., Kapczuk, P., Kupnicka, P., Gawrońska-Szklarz, B., Gutowska, I., Chlubek, D., Baranowska-Bosiacka, I., 2021a. The Effect of Hypoxia on the Expression of CXC Chemokines and CXC Chemokine Receptors-A Review of Literature. Int J Mol Sci 22, 843.
22. Korbecki, J., Simińska, D., Gąssowska-Dobrowolska, M., Listos, J., Gutowska, I., Chlubek, D., Baranowska-Bosiacka, I., 2021b. Chronic and Cycling Hypoxia: Drivers of

Cancer Chronic Inflammation through HIF-1 and NF-κB Activation: A Review of the Molecular Mechanisms. Int J Mol Sci 22, 10701.

23. Lee, B.K., Alexy, T., Wenby, R.B., Meiselman, H.J., 2007. Red blood cell aggregation quantitated via Myrenne aggregometer and yield shear stress. Biorheology 44, 29–35.
24. Li, Y., Zhao, L., Li, X.-F., 2021. Hypoxia and the Tumor Microenvironment. Technol. Cancer Res. Treat. 20, 15330338211036304. https://doi.org/10.1177/15330338211036304
25. Majidpoor, J., Mortezaee, K., 2021a. Angiogenesis as a hallmark of solid tumors - clinical perspectives. Cell. Oncol. 44, 715–737.
26. Majidpoor, J., Mortezaee, K., 2021b. Angiogenesis as a Hallmark of Solid Tumors - Clinical Perspectives 44, 715–737.
27. Metry, G., Adhikarla, R., Schneditz, D., Ronco, C., Levin, N., 2011. Effect of changes in the intravascular volume during hemodialysis on blood viscoelasticity. Indian J. Nephrol. 21, 95.
28. Muravyov, A.V., Bulaeva, S.V., Tikhomirova, I.A., Zamishlayev, A.V., Uzikova, E.V., Miloradov, M.J., 2011. Macro- and microrheological parameters of blood in patients with cerebral and peripheral atherosclerosis: the molecular change mechanisms after pentoxifylline treatment. Clin Hemorheol Microcirc 49, 431–439.
29. Nemeth, N., Deak, A., Szentkereszty, Z., Peto, K., 2018. Effects and influencing factors on hemorheological variables taken into consideration in surgical pathophysiology research. Clin. Hemorheol. Microcirc. 69, 133–140.
30. Nemeth, N., Kiss, F., Miszti-Blasius, K., 2015. Interpretation of osmotic gradient ektacytometry (osmoscan) data: A comparative study for methodological standards. Scand. J. Clin. Lab. Invest. 75, 213–222.
31. Oxburgh, L., 2022. The Extracellular Matrix Environment of Clear Cell Renal Cell Carcinoma. Cancers 14, 4072.
32. Pérez-Tomás, R., Pérez-Guillén, I., 2020. Lactate in the Tumor Microenvironment: An Essential Molecule in Cancer Progression and Treatment. Cancers 12, 3244.
33. Pretorius, E., 2018. Erythrocyte deformability and eryptosis during inflammation, and impaired blood rheology. Clin Hemorheol Microcirc 69, 545–550.
34. Qian, C., Liu, C., Liu, W., Zhou, R., Zhao, L., 2023a. Targeting Vascular Normalization: A Promising Strategy to Improve Immune–vascular Crosstalk in Cancer Immunotherapy 14.
35. Qian, C., Liu, C., Liu, W., Zhou, R., Zhao, L., 2023b. Targeting Vascular Normalization: A Promising Strategy to Improve Immune–vascular Crosstalk in Cancer Immunotherapy 14.

36. Radosinska, J., Vrbjar, N., 2021. Erythrocyte Deformability and Na,K-ATPase Activity in Various Pathophysiological Situations and Their Protection by Selected Nutritional Antioxidants in Humans. Int J Mol Sci 22, 11924.
37. Ruiz, C., Hernandez, G., Andresen, M., Ince, C., Bruhn, A., 2013. Mini-report: Microcirculatory flow abnormalities in a patient with severe hyperviscosity syndrome. Clin. Hemorheol. Microcirc. 54, 33–38.
38. Schaaf, M.B., Garg, A.D., Agostinis, P., 2018. Defining the role of the tumor vasculature in antitumor immunity and immunotherapy. Cell Death Dis. 9, 115.
39. Słoczyńska, K., Kózka, M., Pękala, E., Marchewka, A., Marona, H., 2013. In vitro effect of pentoxifylline and lisofylline on deformability and aggregation of red blood cells from healthy subjects and patients with chronic venous disease. Acta Biochim Pol 60, 129–135.
40. Snipstad, S., Sulheim, E., de Lange Davies, C., Moonen, C., Storm, G., Kiessling, F., Schmid, R., Lammers, T., 2018. Sonopermeation to improve drug delivery to tumors: from fundamental understanding to clinical translation. Expert Opin Drug Deliv 15, 1249–1261.
41. Steele, A.R., Howe, C.A., Gibbons, T.D., Foster, K., Williams, A.M., Caldwell, H.G., Brewster, L.M., Duffy, J., Monteleone, J.A., Subedi, P., Anholm, J.D., Stembridge, M., Ainslie, P.N., Tremblay, J.C., 2024. Hemorheological, cardiorespiratory, and cerebrovascular effects of pentoxifylline following acclimatization to 3,800 m. Am J Physiol Heart Circ Physiol 326, H705–H714.
42. Sugimori, H., Tomoda, F., Koike, T., Kurosaki, H., Masutani, T., Ohara, M., Kagitani, S., Inoue, H., 2013. Increased blood viscosity is associated with reduced renal function and elevated urinary albumin excretion in essential hypertensives without chronic kidney disease. Hypertens Res 36, 247–251.
43. Szabo, J.P., Denes, N., Arato, V., Racz, S., Kis, A., Opposits, G., Kepes, Z., Hajdu, I., Joszai, I., Emri, M., Kertesz, I., Mezo, G., Trencsenyi, G., 2022. In Vivo Imaging of Neo-angiogenesis of Transplanted Metastases in Subrenal Capsule Assay Induced Rat Model. In Vivo 36, 1667–1675.
44. Szentkereszty, Z., Kotan, R., Kiss, F., Klarik, Z., Posan, J., Furka, I., Sapy, P., Miko, I., Peto, K., Nemeth, N., 2014. Effects of various drugs (flunixin, pentoxifylline, enoxaparin) modulating micro-rheological changes in cerulein-induced acute pancreatitis in the rat. Clin. Hemorheol. Microcirc. 57, 303–314.
45. Theek, B., Baues, M., Gremse, F., Pola, R., Pechar, M., Jahnen-Dechent, W., Storm, G., Kiessling, F., Lammers, T., 2018. Histidine-rich glycoprotein-induced vascular

normalization improves EPR-mediated drug targeting to and into tumors. J. Control. Release Off. J. Control. Release Soc. 282, 25–34.

46. Tian, H., Luo, Z., Liu, L., Zheng, M., Chen, Z., Ma, A., Liang, R., Han, Z., Lu, C., Cai, L., 2017. Cancer Cell Membrane-Biomimetic Oxygen Nanocarrier for Breaking Hypoxia-Induced Chemoresistance. Adv. Funct. Mater. 27, 1703197.
47. Trencsenyi, G., Kertai, P., Bako, F., Hunyadi, J., Marian, T., Hargitai, Z., Pocsi, I., Muranyi, E., Hornyak, L., Banfalvi, G., 2009. Renal capsule-parathymic lymph node complex: a new in vivo metastatic model in rats. Anticancer Res. 29, 2121–2126.
48. Tsoneva, I., Semkova, S., Bakalova, R., Zhelev, Z., Nuss, P., Staneva, G., Nikolova, B., 2022. Electroporation, electrochemotherapy and electro-assisted drug delivery in cancer. A state-of-the-art review. Biophys Chem 286, 106819.
49. Turley, R.S., Fontanella, A.N., Padussis, J.C., Toshimitsu, H., Tokuhisa, Y., Cho, E.H., Hanna, G., Beasley, G.M., Augustine, C.K., Dewhirst, M.W., Tyler, D.S., 2012. Bevacizumab-induced alterations in vascular permeability and drug delivery: a novel approach to augment regional chemotherapy for in-transit melanoma. Clin Cancer Res 18, 3328–3339.
50. van Elteren, H.A., Ince, C., Tibboel, D., Reiss, I.K.M., de Jonge, R.C.J., 2015. Cutaneous microcirculation in preterm neonates: comparison between sidestream dark field (SDF) and incident dark field (IDF) imaging. J. Clin. Monit. Comput. 29, 543–548.
51. Vayá, A., Martínez Triguero, M., Ricart, A., Plumé, G., Solves, P., Corella, D., Romagnoli, M., 2009. Erythrocyte aggregability and AB0 blood groups. Clin. Hemorheol. Microcirc. 41, 67–72.
52. Wang, T., Wu, Zhiqiang, Bi, Y., Sun, H., Wu, Zhipeng, Wang, Y., Yan, W., Wei, H., Wang, C., 2020. HIF-1α and HIF-2α Mediated PARVB Expression Promotes Tumor Growth and Metastasis in Malignantmelanoma.
53. Wang, Z.-P., Li, K., Dong, K.-R., Xiao, X.-M., Zheng, S., 2014. Congenital mesoblastic nephroma: Clinical analysis of eight cases and a review of the literature. Oncol. Lett. 8, 2007–2011.
54. Wardman, P., 2007. Chemical radiosensitizers for use in radiotherapy. Clin. Oncol. R. Coll. Radiol. G. B. 19, 397–417.
55. Whatcott, C.J., Han, H., Posner, R.G., Hostetter, G., Von Hoff M, D., 2011. Targeting the tumor microenvironment in cancer: why hyaluronidase deserves a second look. Cancer Discov 1, 291–296.

56. Xu, J., Han, W., Yang, P., Jia, T., Dong, S., Bi, H., Gulzar, A., Yang, D., Gai, S., He, F., Lin, J., Li, C., 2018. Tumor Microenvironment-Responsive Mesoporous MnO2-Coated Upconversion Nanoplatform for Self-Enhanced Tumor Theranostics. Adv. Funct. Mater. 28, 1803804.
57. Yi, M., Jiao, D., Qin, S., Chu, Q., Wu, K., Li, A., 2019. Synergistic effect of immune checkpoint blockade and anti-angiogenesis in cancer treatment. Mol. Cancer 18, 60.
58. You, L., Wu, W., Wang, X., Fang, L., Adam, V., Nepovimova, E., Wu, Q., Kuca, K., 2021. The role of hypoxia-inducible factor 1 in tumor immune evasion. Med. Res. Rev. 41, 1622–1643.

9. Appendix

Ethical approval registration Nr.: 21/2017/UDCAW

9.1. Independent work

- Measurements: Sysmex K-4500 microcell counter
  Myrenne MA-1 aggregometer
- Data processing
- Preparation of the presentation
- Study of the literature background of the research topic, and the theoretical background of measurements.

9.2. Assisted work

- Blood sampling
- Measurements: LoRRca MaxSis osmoscan ektacytometer
  Camera monitoring of renal microcirculation
- Statistical analysis

9.3. Presentations

Ho Quang Tri Vinh: Renal Ne/De tumor cells and related microcirculatory changes in a rat model
Annual University of Debrecen, Medical and Health Science Local Scientific Conference (TDK), 2023
„Experimental surgery, experimental anesthesiology" section

Ho Quang Tri Vinh: Renal Ne/De tumor cells and related microcirculatory changes in a rat model
XVIII. Sántha Kálmán Scientific Roundtable Conference, 2023

9.4. Plagiarism declaration

DECLARATION

I, the undersigned

Ho Quang Tri Vinh (Neptun code:CM0KQ7)

a student of the University of Debrecen, Faculty of Medicine, being fully aware of my legal liability, do thereby declare and certify with my signature that my thesis, entitled

Renal Ne/De tumor cells and related microcirculatory changes in a rat model

is my own original work and that the printed and electronic literature referred to in it was used in accordance with the international rules of copyright.

I understand that in the case of a thesis, it is considered plagiarism when:

- quoting word for word without quotation marks and referring to literature without proper citation.
- referring to content without citing the literature
- presenting previously published ideas of other authers as one's own.

I, the undersigned, declare that I have been informed of the concept of plagiarism. I understand that in case of plagiarism, my research essay will be rejected.

Debrecen, 24 March 2025

……

signature